https://doi.org/10.1016/j.jmapro.2019.05.045

Feasibility investigation on ductile machining of single-crystal silicon for deep micro-structures by ultra-precision fly cutting

Zhanwen Sun, Suet To*, K M Yu

State Key Laboratory in Ultra-precision Machining Technology, Department of Industrial and Systems Engineering, The Hong Kong Polytechnic University, Kowloon, Hong Kong

** Corresponding author at: The Hong Kong Polytechnic University, Department of Industrial and Systems Engineering, State Key Laboratory in Ultra-precision Machining Technology, Kowloon, Hong Kong. Email:* sandy.to@polyu.edu.hk*; Tel: +852 2766 6587; Fax: +852 2764 7657*

Abstract

Single-crystal silicon is a widely used brittle material in infrared optics and optoelectronics industries. However, due to its extremely low fracture toughness, it is difficult to obtain deep micro-structures on single-crystal silicon with ultra-smooth surface quality using previous ductile machining models based on plunge cutting, diamond milling and grinding. Current methods to enhance the machinability of silicon include laser-assisted machining, ion implantation modification and vibration-assisted machining. However, the increase of the ductile machining depth using these methods is still very small in the fabrication of deep micro-structures with a depth over tens of micrometers on silicon. This paper proposes a novel ductile machining model for ultra-precision fly cutting (UPFC) to efficiently fabricate deep micro-structures on silicon. The modeling results show that through configuring a large swing radius, much deeper ductile machining depth can be reached by UPFC. To confirm this proposed model, micro-grooves with different depths were machined, and the surface micro-topographies, form error, tool wear patterns and material phase transformation were analyzed and compared with that acquired by diamond sculpturing method. The experimental results demonstrated that much deeper micro-grooves (over tens of micrometers) with better surface quality were acquired by UPFC. Moreover, compared with the sculpturing method, UPFC prolonged the tool life, and generated less amorphous silicon on the machined surface.

Keywords: ductile machining process; micro-structures; single-crystal silicon; tool wear

1. Introduction

The manufacture of micro-structures on single-crystal silicon has attracted widespread attention for various applications in the advanced infrared (IR) optics, solar cells and photoelectricity industry, due to its unique optical functions, excellent light-trapping performance and improvement of photoelectric conversion efficiency [1-3]. For example, micro-structured surfaces of silicon highly enhance the

photoelectric conversion efficiency of solar cells, compared with smooth surfaces [4]. Micro-lens array of silicon can achieve the integration and minimization of advanced IR optical systems [5]. However, the inherent low fracture toughness of single-crystal silicon significantly limits the attainable depth of the silicon micro-structures without brittle fractures. The ductile machining depth of silicon generally ranges from 90 nm to less than 200 nm [6], so severe brittle fractures and micro-cracks can propagate into the finished surfaces when adopting a large cutting depth. Besides, the original surface of an unprocessed silicon wafer is generally in the shape of plane, which greatly increases the material removal amount for deep micro-structures. Even though both traditional and non-traditional machining methods have been proposed for processing silicon, it is still a difficult task to acquire deep micro-structures on silicon with optically qualified form accuracy.

A few technologies based on the etching process, such as laser-assisted etching and lithography, have been used for the fabrication of silicon micro-structures [7-9]. For example, a type of dry etching method based on the femtosecond laser modification was proposed by Liu et al. [10], to fabricate three dimensional micro-structures on silicon wafers, such as micro gears. However, due to the low machining efficiency and the insufficient machining accuracy, it is difficult for these non-traditional methods to generate deep micro-microstructures on silicon with a sub-micrometric form accuracy and nanometric surface roughness. Further, the geometries and shapes possible to be fabricated by etching methods are very limited.

Ultra-precision mechanical machining technologies, dominated by micro-grinding and diamond cutting technologies, are widely considered to be more promising for the effective generation of micro-structures on brittle materials [11-13]. Through adopting a small depth of cut, ultra-smooth surfaces with high form accuracy can be generated on silicon using ultra-precision machining technologies [14]. However, if the depth of cut is larger than a critical value, the finished surfaces can be very rough due to the propagation of brittle fractures. For example, a set of deep micro-grooves and micro pyramid-structured surfaces were successfully fabricated on silicon by single-point diamond micro-grinding technology [15, 16]. Nevertheless, the surface roughness acquired by this abrasive method is very high at about 200 to 300 nm. More importantly, the abrasive method is quite time-consuming, and the unavoidable subsurface damage induced by the dynamic pressure of the diamond grits highly restrict its practical application on the fabrication of micro-structures on single-crystal silicon.

In contrast, diamond cutting technologies, such as diamond milling, diamond sculpturing and fast

and slow tool serve (FTS/STS), is more flexible in the ductile machining of brittle materials for freeform surfaces and micro-structures [17-20]. By means of slow tool servo, 5.5 μm deep micro-lens arrays were machined on single-crystal silicon by Mukaida et al. [17]. They demonstrated that smooth surfaces with a surface roughness of 4 nm Sa can be achieved under a very small feed rate. After configuring an appropriate title angle of the silicon wafer with respect to the micro-milling tool, Arif et al. [21] successfully fabricated micro-grooves with a depth of 15 μm using end-milling technology. Nevertheless, the surface roughness of these silicon micro-grooves is over 80 nm. As learned from the ductile machining models for milling and slow tool servo, small feed rates and depths of cut need to be carefully selected to suppress the propagation of micro-cracks and brittle fractures onto the finished surfaces [19, 22], which greatly restrict the depth of the micro-structures fabricated on silicon. Consequently, even though smooth surfaces with high form accuracy can be achieved by diamond milling and slow tool servo under a small depth of cut, it is difficult for these methods to fabricate deep micro-structures without brittle fractures on silicon.

Diamond sculpturing method was successfully applied in the manufacture of micro-structures on silicon by restricting the instantaneous cutting depth within the critical depth of cut (DoC) of silicon. The major advantage of sculpturing method is its feasibility of fabricating micro-structures with very high resolution. By means of sculpturing method, 0.1 μm deep micro-grooves with a 11 nm roughness were obtained by Chen et al. [23]. However, due to the extremely small critical DoC of silicon (normally ranging from 100 nm to 200 nm [24]), it is difficult for diamond sculpturing method to generate deep microstructures with a depth over tens of micrometers. To enhance the machinability of single-crystal silicon, a few technologies, such as laser-assisted cutting [25], ion implantation modification [6] and vibration-assisted machining [26, 27], were successfully integrated into the diamond sculpturing method by increasing the critical DoC. Assisted by ultrasonic elliptical vibration, the ductile machining depth of the micro-structures was increased to 1 μm by Zhang et al. [28] with better surface quality. In addition, as reported by Xiao et al. [6], higher critical DoC of silicon (2 μm) was observed after modifying the silicon surface by ion implantation, which is beneficial to the ductile machining micro-grooves. However, the increase of the ductile machining depth by these methods is still very small for deep micro-structures with a depth over tens of micrometers. Up to date, very little research focuses on the ductile machining of silicon for micro-structures with a depth over 20 μm.

Ultra-precision fly cutting (UPFC) is a very flexible machining technology for micro-structures with

intricated shapes [29, 30]. Because of its unique cutting process, the ductile machining model for UPFC is totally different from that of diamond milling, diamond sculpturing and FTS/STS. Previous investigation on UPFC of brittle materials mostly performed under a very small depth of cut (less than 10 μm) [31, 32]. Nevertheless, literature on the ductile machining of silicon using UPFC under large depths of cut is very limited. More importantly, the feasibility of UPFC in fabricating deep micro-structures (over tens of micrometers) in ductile mode on brittle materials was not yet well demonstrated. This study theoretically and experimentally demonstrates the feasibility of UPFC in fabricating deep micro-structures on silicon in ductile mode. The effects of machining parameters (i.e., feed rate and depth of cut) on the ductile machining depth of UPFC were discussed. This research result offers a feasible solution for the ductile machining of single-crystal silicon or other hard and brittle materials for deep micro-structures.

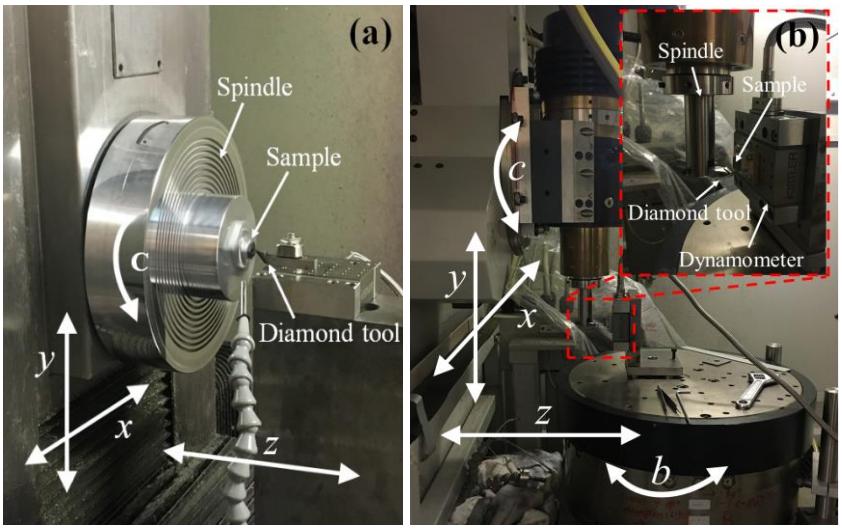

Fig. 1. Hardware configuration of the (a) diamond sculpturing method and (b) UPFC.

2. Experimental setup

A set of taper grooves with increasing cutting depth were fabricated on single-crystal silicon using UPFC and sculpturing, respectively. The tilt angle of each taper groove was fixed at 0.1°, and both <110> and <100> directions were selected. As shown in Fig. 1 (a), an ultra-precision freeform machining system (Moore Nanotech 350FG) with three linear axes and an air bearing spindle was used for the diamond sculpturing method. The diamond tool was configured on the *z*-axis, and the silicon wafer was fixed on the spindle by a fixture. Through feeding the diamond tool upwards with a title angel, taper grooves with increasing cutting depth can be generated on the wafer. As shown in Fig. 1 (b), a 5-axes freeform milling

system (Precitech 705G) was applied in UPFC of taper grooves on silicon. The silicon wafer glued on a fixture was fixed on the *b*-axis, and a diamond tool was mounted on the high-speed spindle. The taper grooves were machined by the horizontally feeding motion of the spindle for UPFC. Table 1. shows the machining parameters for diamond sculpturing and UPFC in the machining of taper grooves.

Table 1. Machining parameters for diamond sculpturing and UPFC.

Machining parameters	UPFC	Diamond sculpturing
Swing radius (mm)	40.5	none
Cutting speed (m/s)	8.4	0.004
Spindle rotation (rpm)	2000	none
Feed rate (μm/r)	3	none
Feed directions	<110>, <100>	<110>, <100>
Atmosphere	Dry	Dry

Table 2. Machining parameters in UPFC of micro-grooves.

Machining parameters	UPFC	Diamond sculpturing
Swing radius (mm)	40.5	none
Cutting speed (m/s)	12.6	0.004
Spindle rotation (rpm)	3000	none
Feed rate (μm/r)	3	none
Depth of cut (μm)	10, 20, 30	3, 6, 9
Feed directions	<100>	<100>
Atmosphere	Dry	Dry

In addition, micro-grooves of different depths were fabricated in the <100> direction of single-crystal silicon by UPFC and sculpturing method, respectively. The machining parameters is shown in Table 2. The machining strategy of UPFC is illustrated in Fig. 2, in which the rotating spindle carries the diamond tool, feeding in *x* direction with the presetting depth of cut, so arc-shaped micro-grooves are formed due to the imprint of the diamond tool profile. It worth to note that the cutting direction of UPFC remains constant in relation to the crystallization direction of single-crystal silicon. For sculpturing method, deep micro-grooves cannot be directly fabricated using large depths of cut. Thus, deep micro-grooves were generated using the periodical sculpturing operation of the workpiece surface, with each single cutting cycle performed under a depth of cut of about 100 nm, until reaching the desired depth, to suppress the propagation of micro-cracks.

Two diamond tools with the same round nose radius of 0.5 mm were used in the experiments of

sculpturing and UPFC. The rake angle of the diamond tool is -25°, while the clearance angle is 10°. An optical microscope BX60 provided by Olympus corporation was used to acquire the microscopies of the micro-grooves. Further, a three-dimensional non-contact optical measurement system provided by Zygo Corporation was applied to capture the corresponding micro-topographies. A scanning electron microscope was used to observe the tool wear patterns. A LabRAM 800 Raman Spectrometer was used to analysis the material phase transformation of the finished surfaces.

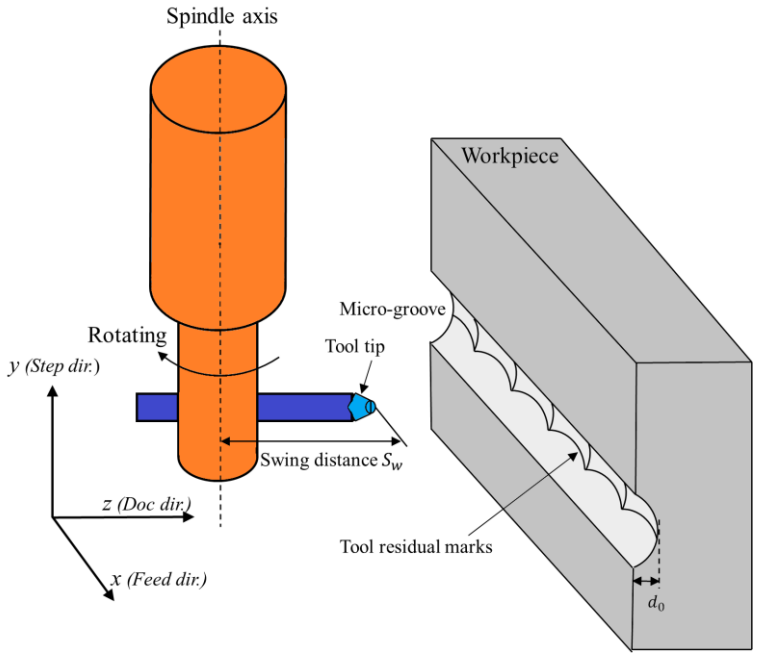

Fig. 2. Schematic illustration of machining principle in UPFC of micro-grooves.

3. Ductile machining model

The machining principle of UPFC for micro-grooves is illustrated in Fig. 2. A diamond tool is fixed on the high-speed spindle with a specific swing radius (S_w) that is defined as the maximum distance between the tool tip and the rotational central line of the spindle. During the machining process, the rotating spindle horizontally feeds in the x direction, and the diamond tool intermittently cuts into and out of the workpiece surface with a specific depth of cut (d_0). Then, a micro-groove can be formed on the workpiece surface with its cross-sectional profile totally the same as the geometrical shape of the tool edge. It worth to note that more complicated micro-structures, such as micro-pyramid arrays, can be acquired by UPFC through adding another rotational axis on the workpiece. Due to this unique cutting process of UPFC, its ductile machining mechanism is different from that of milling, grinding and FTS/STS.

The schematic of the 3D chip morphology in fly grooving is shown in Fig. 3. In fly grooving, each chip is generated by the two intermittent cutting steps, namely previous rotary cutting and current rotary cutting. Therefore, the chips are enveloped by the initial surface of the workpiece, the top surface formed by previous rotary cutting and the bottom surface formed by current rotary cutting, as shown in Fig. 3. As there is no step movement in fly grooving, the chips are axisymmetric. The point *a* is the midpoint of line *de*, while points *b* and *c* are the peak point of the curves *cbe* and *dce*, respectively. Actually, the chip morphology is axisymmetric in the step direction, the points *a*, *b* and *c* are the intersection points between the central plane and the enveloped surfaces of the chip, as denoted by the yellow lines in Fig. 3. From the geometric knowledge, it is known that even though the chip thickness changes in both the feed and step directions, the thickest chip thickness is distributed in the central plane of the chips.

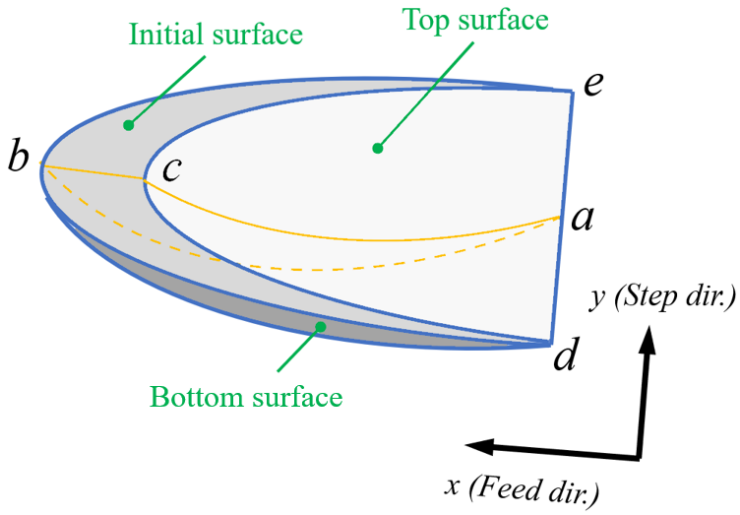

Fig. 3. Schematic illustration of the chip morphology for UPFC and TTSD.

In order to obtain ultra-smooth surfaces on both the sides and the bottom of the micro-grooves, no brittle fractures are allowed to be generated during the whole chip formation duration. It is known that brittle fractures generate and propagate on the condition that the instantaneous chip thickness exceeds the critical depth of cut of silicon [33]. Thus, based on the schematic 3D chip morphology of UPFC, as shown in Fig. 3, it is learned that even though the chip thickness changes in both the feed and step directions, the thickest thickness in the step direction (TTSD), distributed in the central plane of the chips, plays a crucial role on the first occurrence of brittle fractures.

It is learned from Fig. 4 that the TTSD values change in the feed direction with tool rotation. Therefore, in order to the learn the ductile machining mechanism for UPFC, the TTSD values at different

rotation angles, denoted as h_θ, need to be calculated. As shown in Fig. 4, a system of rectangular coordinates (*o*-*xyz*) is defined at the crossing point of the diamond tool holder and the spindle rotational axis, with the *x* axis coincident with the feed direction. As the chip formation duration is extremely short in UPFC, it is assumed that the spindle is stationary in the chip formation duration when calculating TTSDs.

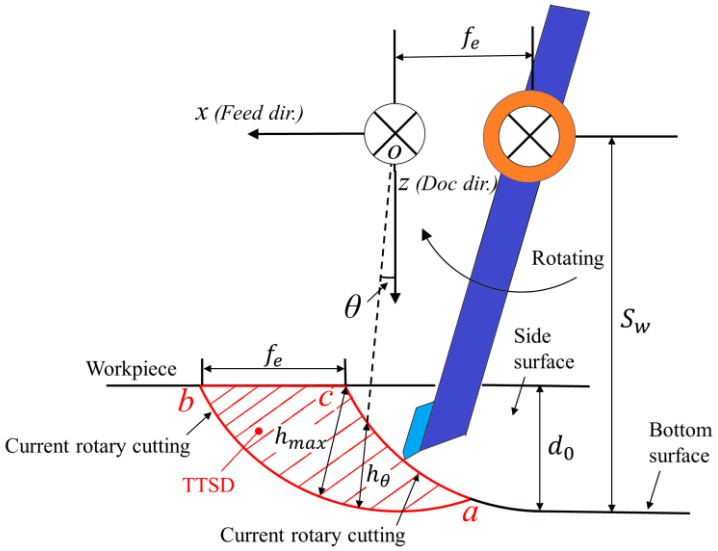

Fig. 4. Schematic of UPFC viewed along the *y* direction.

For the curve formed by the previous rotary cutting, its boundary points include points *a* and *c*, whose mathematical expression is given by

$$(x + f_e)^2 + z^2 = {S_w}^2 \tag{1}$$

where f_e denotes the feed rate in mm/r.

For the curve generated by the current rotary cutting, its boundary points include points *a* and *b*, whose mathematical expression is given by

$$x^2 + z^2 = {S_w}^2 \tag{2}$$

For the curve describing the original surface, its boundary points include points *b* and *c*, which can be expressed as

$$\mathrm{z} = S_w - d_0 \tag{3}$$

where d_0 is the depth of cut equal to the depth of the machined micro-groove.

Based on the geometry relation, point *a* is located in the middle of the two consecutive rotational centers, as shown in Fig. 4. Thus, according to Eq. (1), the coordinate components of point *a* can be

expressed as

$$\begin{cases} x_a = -\frac{f_e}{2} \\ z_a = \sqrt{{S_w}^2 - {f_e}^2/4} \end{cases} \tag{4}$$

Points *b* and *c* are located at the original surface, as shown in Fig. 4. For point *b*, according to Eq. (2) and (3), its coordinate components can be expressed as

$$\begin{cases} x_b = \sqrt{{S_w}^2 - (S_w - d_0)^2} - f_e \\ z_b = S_w - d_0 \end{cases} \tag{5}$$

Similarly, for point *c*, its coordinate components can be expressed as

$$\begin{cases} x_c = \sqrt{{S_w}^2 - (S_w - d_0)^2} \\ z_c = S_w - d_0 \end{cases} \tag{6}$$

Therefore, using Eq. (1), Eq. (4) and Eq. (6), any point (x_0, z_0) on the curve formed by the previous rotary cutting can be denoted as follows:

$$\begin{cases} x_a \le x_0 < x_c \\ z_0 = \sqrt{{S_w}^2 - (x + f_e)^2} \end{cases} \tag{7}$$

According to Eq. (3), Eq. (4) and Eq. (6), any point (x_0, z_0) on the curve generated by the current rotary cutting is denoted as follows:

$$\begin{cases} x_c \le x_0 < x_b \\ z_0 = S_w - d_0 \end{cases} \tag{8}$$

The line passing through the point (x_0, z_0) and the origin point (0, 0) of the defined coordinate system *o-xyz* can be expressed as

$$\frac{x}{x_0} = \frac{z}{z_0} \tag{9}$$

Because of the rotational trajectory of the diamond tool, TTSDs refer to the distance from the point (x_0, z_0) to the intersection point (x_1, z_1) between the line expressed in Eq. (9) and the curve expressed in Eq. (2), which can be given as

$$\begin{cases} x_1 = \sqrt{\frac{{x_0}^2 \cdot {S_w}^2}{{x_0}^2 + {z_0}^2}} \\ z_1 = \sqrt{\frac{{z_0}^2 \cdot {S_w}^2}{{x_0}^2 + {z_0}^2}} \end{cases} \tag{10}$$

In total, the TTSD value (h_θ) at a rotation angle (θ) is essentially equal to the distance between the point (x_0, z_0) and point (x_1, z_1), which can be calculated as

$$h_\theta = \sqrt{(x_1 - x_0)^2 + (z_1 - z_0)^2} \tag{11}$$

Therefore, from the expression of h_θ, it is learned that TTSD is not only influenced by the depth of cut (d_0), but also is a function of the configured swing radius (S_w). This special mathematical relation leads to an extremely small chip thickness under a large swing radius in UPFC, even when machining with large feed rates and cutting depths, accordingly ensuring the ductile machining of deep micro-grooves on single-crystal silicon.

4. Results and discussion

4.1 Effect of machining parameters on ductile-brittle transition in UPFC

As learned from the model, ductile-brittle transition happens at the points where the TTSD values exceeds the critical depth of cut (DoC) of silicon. Thus, in order to acquire a smooth surface in UPFC, TTSD values need to be lower than the critical DoC to ensure the ductile material removal of silicon. Fig. 5 (a) and (b) show the variations of TTSDs with tool rotation at different feed rates and depths of cut. For each tool rotation cycle, TTSDs firstly increase and then decrease after reaching the highest point (the maximum chip thickness). This varying trend exactly reflects the chip formation process of UPFC within each tool rotation, as illustrated in Fig. 4. More specifically, the chip thickness approaches zero at the tool entering point (point *a*), and after increasing to the maximum chip thickness at point *c*, it reduces back to zero again at the tool departing point (point *b*). As a result, if the maximum chip thickness at point *c* is lower than the critical DoC of silicon, no brittle fractures will generate in the cutting process.

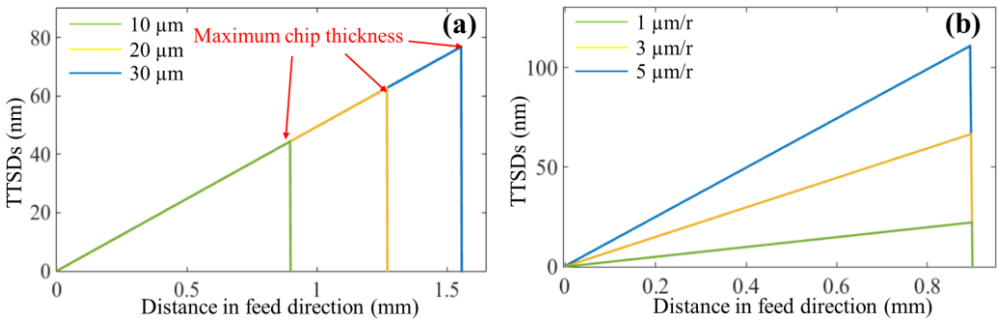

Fig. 5. Variation of TTSD values under (a) different depths of cut and (b) feed rates.

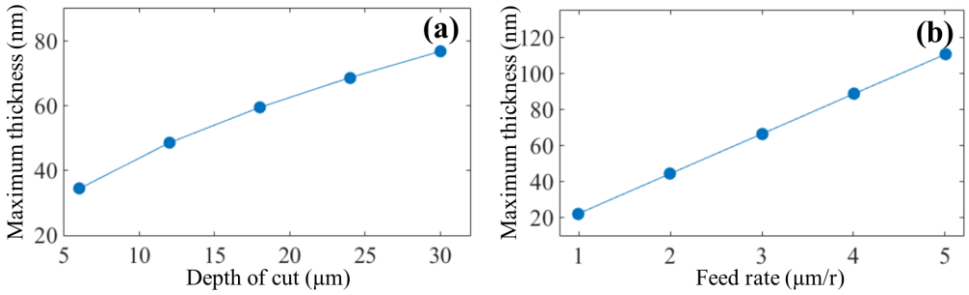

Fig. 6. Maximum chip thickness under different (a) depths of cut and (b) feed rates.

The changes of the maximum chip thickness with increasing depths of cut is illustrated in Fig. 6 (a). The maximum chip thickness with a cutting depth of 30 μm is calculated at nearly 76 nm, which is much less that the critical DoC of silicon at 100~182 nm [6]. Meanwhile, the maximum chip thickness with the feed rates of 3 μm/r and 5 μm/r (calculated at 66 nm and 110 nm) are still less than the critical DoC of silicon, as shown in Fig. 6 (b). As learned from the proposed model, the extremely small chip thickness of UPFC, even under large depths of cut and feed rates, majorly results from the unique machining strategy of UPFC, in which the diamond tool rotates with a large swing radius in the normal plane of the workpiece surface. This unique cutting trajectory leads to the inverse proportional relation between the chip thickness and the swing radius, as expressed in Eq. (11). Based on this mathematical relation, it is found that through configuring a large swing radius in UPFC, the chip thickness will be reduced to an extremely small value even under large feed rates and depths of cut, thereby ensuring the ductile machining of silicon for deep micro-structures without brittle fractures. In contrast, the instantaneous chip thickness of diamond sculpturing is nearly equivalent to the depth of cut, as the schematic of the sculpturing method shown in Fig. 7. Consequently, the depth of cut for diamond sculpturing operation needs to be restricted within the critical DoC of silicon, to avoid the occurrence of brittle fractures. Deep micro-structures can be obtained by periodically plunge cutting operation, as shown in Fig. 7.

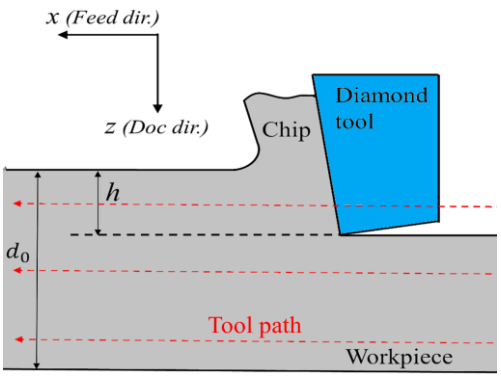

Fig. 7. Schematic illustration of the sculpturing machining process.

4.2 Taper grooves

To validate the advantage of UPFC in achieving deep ductile machining depth on silicon, taper micro-grooves with increasing depth were fabricated by UPFC and diamond sculpturing method, respectively, on single-crystal silicon in the <100> crystal direction. The surface topographies of the taper grooves are shown in Fig. 8. Clear ductile-brittle transitional boundaries can be observed on the optical microscopy and 3D topography of the taper grooves generated by the sculpturing method, as shown in Fig. 8 (a) and (c). The ductile-cut region of diamond sculpturing is quite smooth, while the brittle-cut region presents an obvious rough appearance with bulk cleavages and random fractures. The depth of the transitional point is measured at 148 nm, as illustrated in Fig. 8 (e). This is because the instantaneous chip thickness of diamond sculpturing is nearly equivalent to the depth of cut, so brittle fractures generate at the locations where the depth of cut exceeds the critical DoC of silicon. As a result, the instantaneous cutting depth of sculpturing method need to be lower than the critical DoC of silicon when machining micro-structures, in order to obtain smooth surfaces without brittle fractures on silicon. Nevertheless, due to the extremely low critical DoC of silicon, it is difficult to fabricate deep micro-structures with a depth over tens of micrometers using this method.

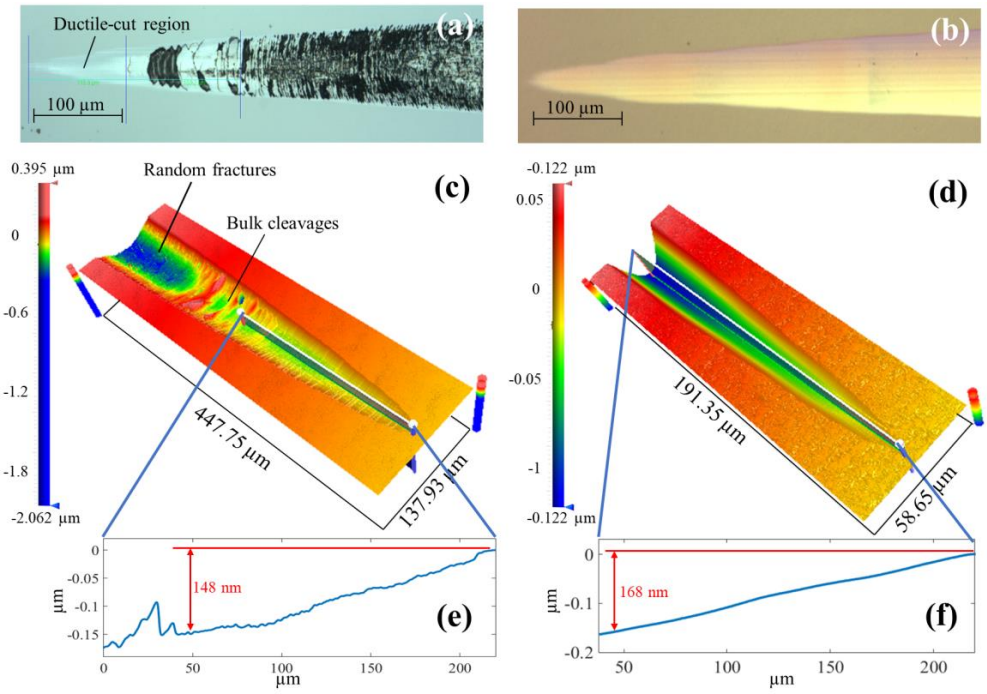

Fig. 8. The optical microscopy, 3D topography and the central profile of the taper groove in <100> direction fabricated by sculpturing method with (a), (c) and (e) and by UPFC with (b), (d) and (f).

In contrast, as shown in Fig. 8 (b) and (d), only smooth surface without cleavages or fractures was observed on the taper groove generated by UPFC, indicating the ductile material removal in UPFC. Besides, the central line profile of the taper groove generated by UPFC is even smoother than that acquired by the sculpturing method, as shown in Fig. 8 (e) and (f). As learned from the ductile machining model for UPFC, this deeper and smoother ductile-cut region generated by UPFC majorly results from its unique rotational cutting trajectory with a large swing radius, which leads to an extremely small chip thickness even under a large depth of cut. Taking advantage of this unique cutting operation of UPFC, ductile material removal of silicon can be ensured despite of the increasing depth of cut. Without loss of generality, similar experiments were conducted in another crystal direction <100>, as shown in Fig. 9. Similar to the results in <100> direction, smoother surface quality as well as deeper ductile cut region are achieved by fly cutting compared with sculpturing, as shown in Fig. 9 (d) and (f).

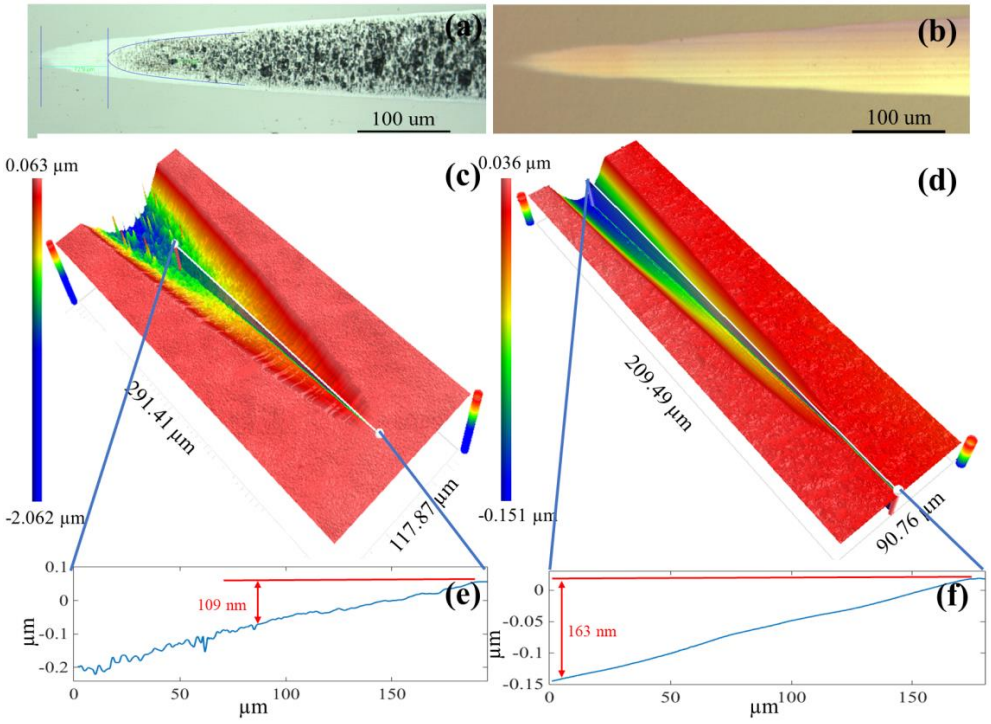

Fig. 9. The optical microscopy, 3D topography and the central profile of the taper groove in <110> direction fabricated by sculpturing method with (a), (c) and (e) and by UPFC with (b), (d) and (f).

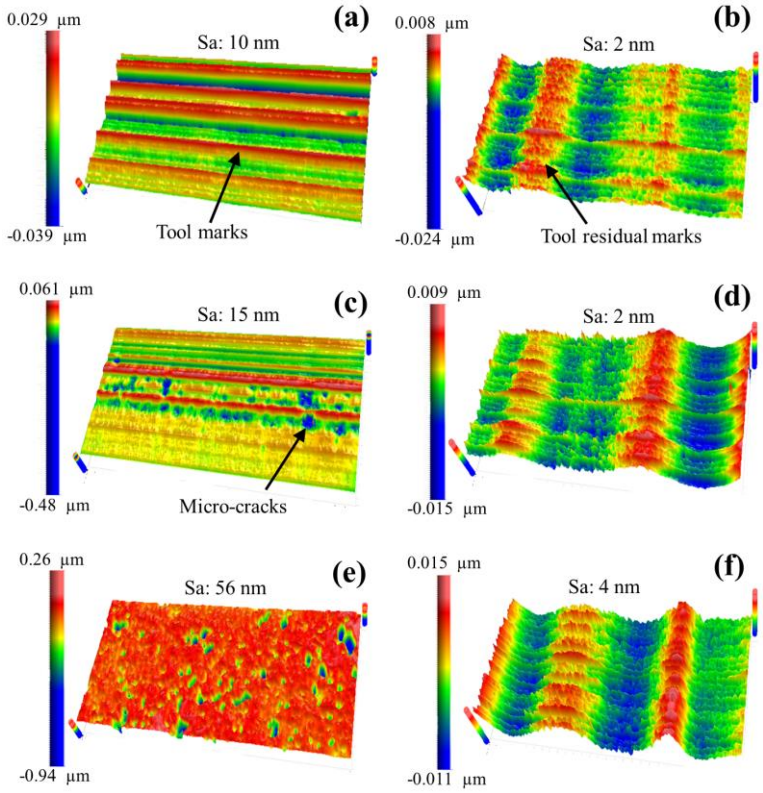

Fig. 10. The bottom-surface micro-topographies of the (a) 3 μm, (c) 6 μm and (e) 9 μm deep micro-grooves machined by sculpturing method, and (b) 10 μm, (d) 20 μm and (f) 30 μm deep micro-grooves machined by UPFC.

4.3 Micro-grooves

The micro-topographies of the micro-grooves generated by sculpturing and UPFC at different depths are shown in Fig. 10. For the sculpturing method, a smooth surface coupled with parallel tool marks in the feed direction was observed on the finished surface of the 3 μm deep micro-groove, as shown in Fig. 10 (a), indicating the ductile material removal process. No brittle fractures were generated in this case due to the periodical plunge operations with each single cutting cycle conducted under a cutting depth of 100 nm, as schematically illustrated in Fig. 7. Nevertheless, when the depth of the sculptured micro-grooves reached 6 μm, intensive micro-cracks were generated along the center line, as shown in Fig. 10 (c). Furthermore, these micro-cracks increased in number and propagated into nearly the whole finished surface of the 9 μm deep micro-groove, as shown in Fig. 10 (e), indicating the dominance of the brittle machining model in this case. This can be more clearly seen from the 3D topography and the cross-sectional profile of the 9 μm deep sculptured micro-groove, as shown in Fig. 11 (a). The increasing propagation of the micro-cracks at deeper micro-grooves generated by the sculpturing method is attributed to the dislocations of the subsurface damage and the micro-cracks

induced by the repetitious plunge cutting operations [33]. Therefore, the experimental results indicate that it is difficult to obtain deep micro-structures without fractures on silicon by diamond sculpturing method.

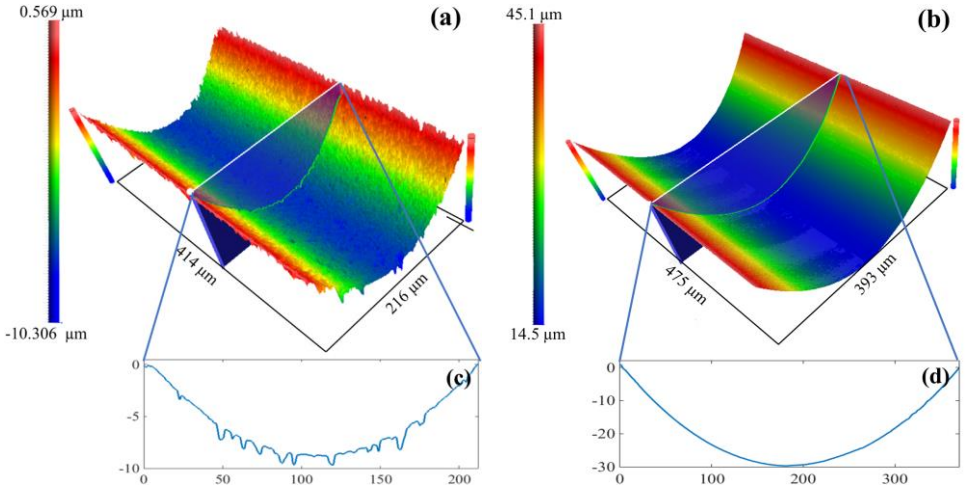

Fig. 11. 3D topography and the corresponding cross-sectional profile of (a) the 9 µm deep sculptured micro-groove and (b) 30 µm deep micro-groove machined by UPFC.

For UPFC, the micro-topographies of the micro-grooves are characterized as stripe patterns that are vertical in relation to the feed direction, which results from the tool residual marks. Interestingly, different from the sculpturing results, no brittle factures or cracks were generated in UPFC even under a much larger cutting depth, from 10 µm to 30 µm, as shown in Fig. 10 (b), (d) and (e). Moreover, for UPFC, the surface roughness at different cutting depths almost remains constant, ranging from 2 nm Sa to 4 nm Sa. This is because the influence of the increasing depth of cut on the maximum chip thickness of UPFC is very small, as illustrated in Fig. 3. For example, the increased value of the maximum chip thickness for UPFC with the cutting depth changing from 10 µm to 30 µm is less than 20 nm, which can be neglected in comparison with the depth of cut. The 3D topography of the 30 µm deep micro-grooves with a smooth arc-shaped cross-sectional profile is shown in Fig. 11 (b), so UPFC is more feasible for the ductile machining of deep micro-grooves with smooth surface quality.

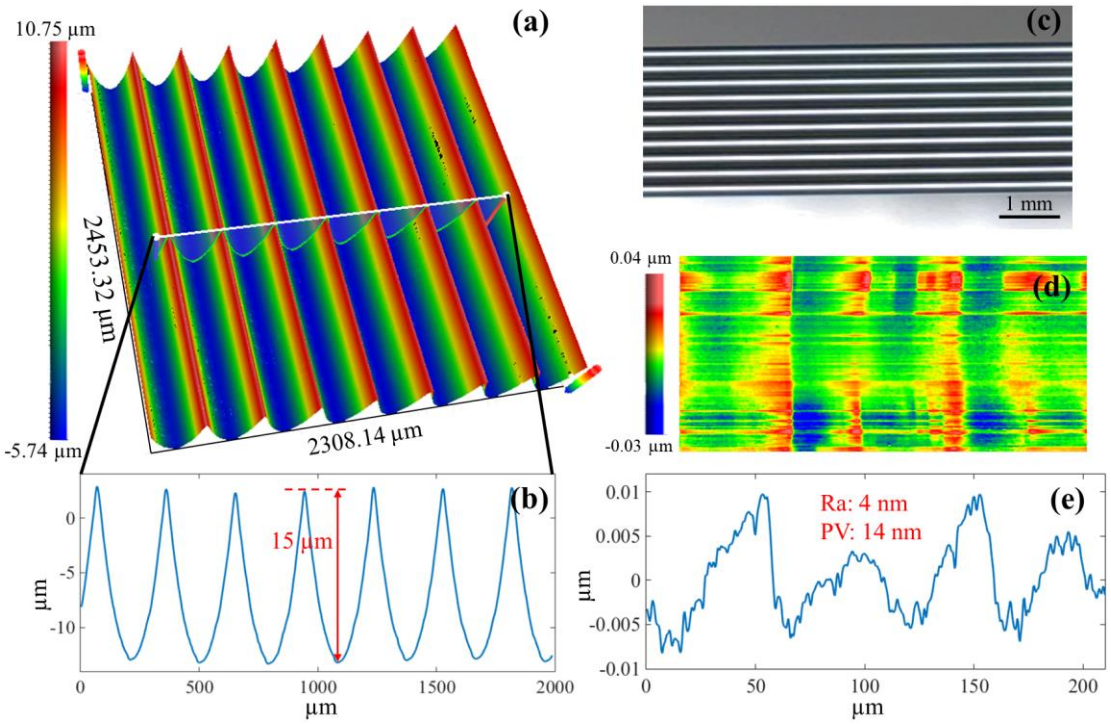

Fig. 12. 15 μm deep micro-raster composed by arc-shaped micro-grooves in <100> direction: (a) 3D surface topography, (b) cross-sectional profile, (c) optical microscope, (d) planarized surface topography and (e) bottom surface profile along feed direction.

Fig. 12 (a) and (b) illustrate the 3D topography and the cross-sectional profile of the optical micro-raster composed of 15 μm deep arc-shaped micro-grooves fabricated by UPFC on single-crystal silicon. From the optical microscopy shown in Fig. 12 (c), an ultra-smooth finished surface can be observed. To validate the IR optical performance, surface roughness and form error were further analyzed as follows. According to Harvey et al. [34], the surface roughness of an optical component is associated with the index named total integrated scattering (TIS), which is necessarily smaller than 0.01 for most IR optical systems. TIS can be expressed as [34]:

$$\mathrm{TIS} \approx \left(\frac{4\pi\delta}{\lambda}\right)^2 \tag{11}$$

where λ is the incident light wavelength and δ denotes the RMS surface roughness Rq. As single-crystal silicon is normally used in IR optical area that transmits the light with wavelength ranging from 1.2 μm to 6 μm, the surface roughness is required to less than 10 nm Rq. To simplify the calculation, the required Ra is estimated as 0.8 that of Rq, so surface roughness lower than 8 nm Ra is required for the IR optical components made by single-crystal silicon. The surface roughness of the raster is measured at 4 nm Ra, as shown in Fig. 12 (e), fulfilling the highest requirement of IR application.

To fulfill the optical application, the maximum allowable form error of an optical element is λ/4 of the transmitted light [35]. As a result, the required form error for a silicon micro-groove needs to be less than 300 nm PV for a 1.2 μm wavelength, in order to avoid the distortion of the gathered profile. Even though the finished surface of UPFC is characterized with stipe patterns, as shown in Fig. 12 (d), the form error fulfils the requirement of silicon optical components for IR applications over the whole range of infrared wavelengths.

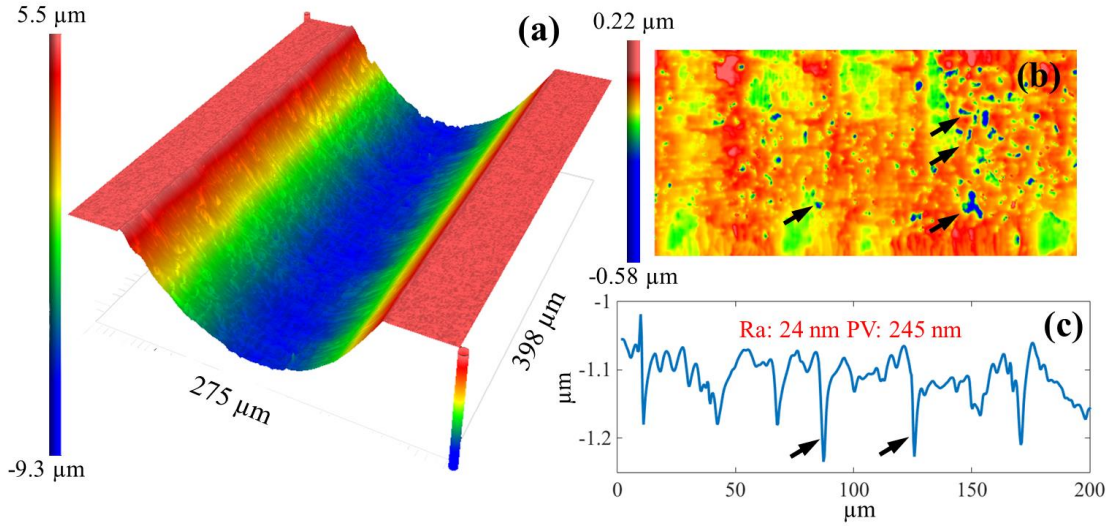

Fig. 13. The 15 μm deep micro-groove machined by fly cutting with a swing radius of 11.4 mm: (a) 3D topography, (b) planarized surface topography and (c) bottom surface profile along feed direction.

According to the proposed model, through configuring a large swing radius for fly cutting, the chip thickness will be reduced to an extremely small value even under large feed rates and depths of cut, thereby ensuring the ductile material removal of silicon for deep micro-structures. To further determine the effect of the swing radius on the ductile cutting performance of fly cutting, a much smaller swing radius of 10.4 mm is adopted in fly cutting of micro-grooves, and the results is shown in Fig. 13. As shown in Fig. 13 (a) and (b), intensive brittle fractures and micro-cracks can be observed on both the 3D surface topography and the planarized surface of the micro-groove generated by fly cutting with small swing radius. These brittle fractures are induced by the large chip thickness under small swing radius. Specifically, with the same feed rate and depth of cut, the maximum chip thickness for 40.5 mm swing radius is only 81 nm, while the maximum chip thickness for 10.4 mm swing radius is over 189 nm. These brittle fractures highly destroy the finished surface quality and lead to the very rugged surface profile as shown in Fig. 13 (c). The

surface roughness and the form error of the micro-groove are measured at 24 nm and 245 nm, respectively, which are also much higher than that acquired by fly cutting with larger swing radius as shown in Fig. 12 (e). Overall, through comparing the results acquired by fly cutting with different swing radiuses, it is validated that better ductile cutting performance is achieved by larger swing radius, which is well accordance with the results of the proposed model.

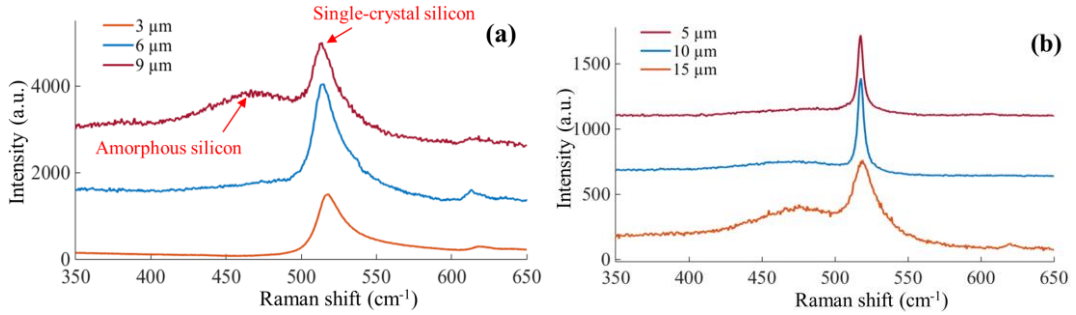

Fig. 14. Raman spectrum of the micro-grooves fabricated using (a) sculpturing method (b) and UPFC with different cutting depths.

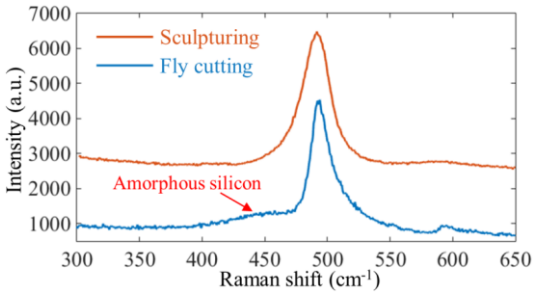

Fig. 15. Raman spectrum of the chips generated by sculpturing and fly cutting.

4.4 Material phase transformation

In the ductile machining of silicon by diamond tools, the high pressure phase transformation (HPPT) inevitably leads to the metallization of brittle materials [33]. For silicon, it has been reported that Si-I (brittle) will transform to Si-II (ductile) under the loading process, then further transform to an amorphous state during the rapid uploading operation [14]. As amorphous silicon influences the performance of the IR components [17], the material phase transformation of silicon should be analyzed for both sculpturing method and UPFC, respectively.

Fig. 14 (a) shows the Raman spectrum of the finished surfaces acquired by the sculpturing method at different depths. A large amount of amorphous silicon was detected on the finished surface at 3 μm, while, interestingly, the ratio of the amorphous silicon was obviously reduced for 6 μm and 9 μm deep micro-grooves. According to Yan et al. [28, 36], the Raman intensity ratio of amorphous silicon is defined

as I_a/I_c, where I_a is the total Raman intensity of amorphous silicon and I_c is the total Raman intensity of crystalline silicon. The value of the Raman intensity ratio can be calculated by integrating method based on the acquired Raman spectrum [36]. In the revised manuscript, the definition of the Raman intensity ratio of amorphous silicon is added. This lower ratio of amorphous silicon at large depth of cut indicates the increasingly dominant brittle material removal mechanism. This observation is well in accordance with the increasing number of micro-cracks observed on the finished surface at higher cutting depths by the sculpturing method, as shown in Fig. 10 (a), (c) and (e). Actually, based on multiple sculpturing experiments, it is difficult to acquire totally fracture-free micro-grooves with a depth of 6 μm on single-crystal silicon by the diamond sculpturing method.

For UPFC, the ratio of the amorphous silicon is much lower than that of sculpturing, as shown in Fig. 14 (b), even under much larger depths of cut from 10 μm to 20 μm. The smoother surface quality as well as less amorphous silicon left on the finished surface by UPFC indicates better optical performance [17]. Furthermore, the ratio of the amorphous silicon is almost unchanged from 5 μm to 10 μm, because the change of the chip thickness, less than 25 nm, is very small at lower cutting depths. However, this ratio significantly increased at the 15 μm deep micro-groove. This increased ratio is probably induced by the large increase of the cutting force as well as the increase of the contacting region between the diamond tool and the silicon in this case. The analysis of the material transformation suggests the advantages of UPFC in obtaining deep arc-shaped grooves with smooth surfaces and with less amorphous silicon.

As known from previous studies, ductile mode cutting of single-crystal silicon is associated with phase transformation caused by high pressure in the cutting region [28]. In diamond sculpturing of silicon, the diamond tool remains in contact with the workpiece surface, so the generated amorphous silicon tends to be left on the finished surfaces and form an amorphous layer. In this case, a broadband peak near 470 cm^{-1} can be observed on the Raman spectrum for 3 μm deep micro-grooves, as shown in Fig. 14 (a). With increasing depth of cut for sculpturing, the material removal mechanism transforms from ductile to brittle, so the peak near 470 cm^{-1} disappears for deep micro-grooves and intensive brittle fractures can be observed on the finished surfaces.

Different from sculpturing, fly cutting removes the material in an intermittently way. Due to the rotary cutting trajectory of the diamond tool, the generated amorphous silicon is more easily to be removed in the form of chips. Accordingly, less amorphous silicon is left on the finished surface even

though machining in ductile mode. This can be validated by the Raman spectrum of the chips generated in fly cutting of 5 μm deep micro-grooves, as shown in Fig. 15. As shown in Fig. 15, the broadband peak near 470 cm^{-1} indicates the existence of amorphous silicon on the chips. Thus, even though less or no amorphous silicon is observed on the finished surfaces in fly cutting, the amorphous silicon observed on the chips also demonstrates the ductile material removal mode in fly cutting. In contrast, as shown in Fig. 14 (a) and Fig. 15, no amorphous silicon can be observed on both finished surfaces and generated chips in sculpturing of 9 μm deep micro-grooves, indicating the totally brittle material removal mode of sculpturing.

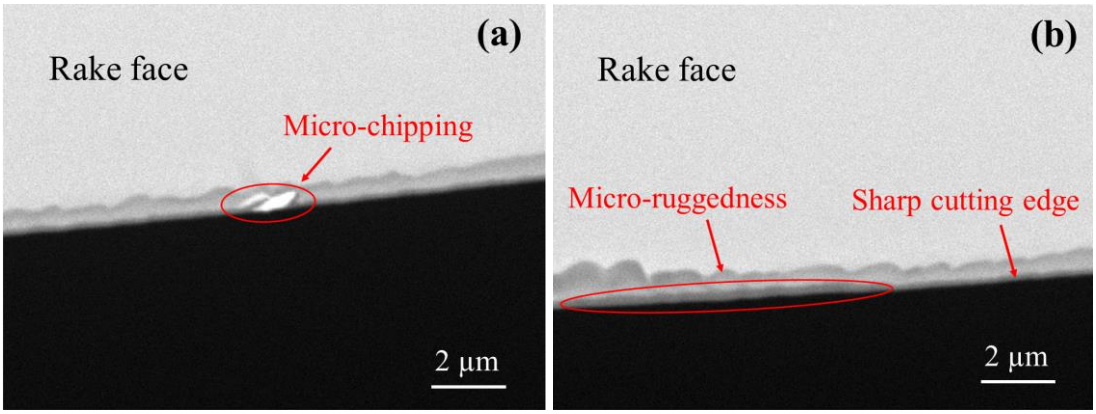

Fig. 16. Tool wear patterns after a cutting distance of (a) 200 m for sculpturing method and (b) 700 m for UPFC.

4.5 Tool wear

Fig. 16 (a) and (b) compare the different tool wear patterns for the diamond sculpturing method and UPFC under dry cutting operation on single-crystal silicon. In the tool wear test for sculpturing, the cutting depth was fixed at 100 nm. After sculpturing the silicon wafer for 200 m with a fixed cutting depth of 100 nm, the tool rake face was observed by SEM, as shown in Fig. 16 (a). The main reason for setting the cutting depth at 100 nm is to suppress the propagation of brittle fractures. It is known that brittle fractures can extensively generate and destroy the finished surfaces when the cutting depth reaches the critical depth of cut of silicon (~120 nm) [6]. As shown in Fig. 16 (a), obvious micro-chipping was formed on the apex of the diamond tool after cutting about 200 m using diamond sculpturing. The earlier occurrence of the micro-chipping on the tool apex majorly result from the frequent brittle impact on the apex of the diamond tool, As the brittle machining mode is dominant during sculpturing of deep grooves on silicon. In addition, this micro-chipping can imprint on the finished surface during the machining

process, and results in ‘bridge marks’ on the bottom surface of the micro-grooves along the cutting direction, as shown in Fig. 17 (a).

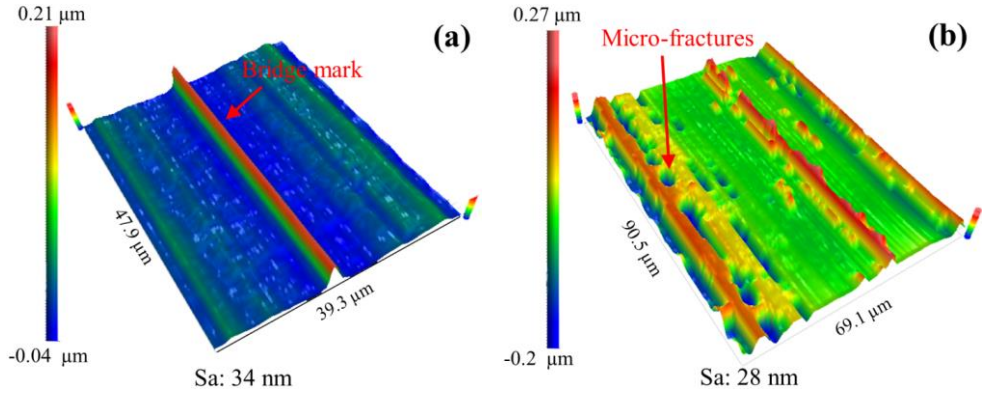

Fig. 17. The damage of the finished surface caused by tool wear for (a) sculpturing and (b) UPFC.

In the tool wear test for fly cutting, the cutting depth and the cutting distance were set at 9 μm and 700 m, respectively. Namely, the tool wear pattern of fly cutting was observed after cutting a distance of 700 m with a fixed cutting depth of 9 μm, as shown in Fig. 16 (b). UPFC presents another kind of tool wear pattern characterized as micro-ruggedness of the cutting edge after a much longer cutting distance of about 700 m compared with the sculpting method. The different tool wear patterns between diamond sculpturing and UPFC majorly results from the different cutting mechanisms dominated in the cutting process. More specifically, in UPFC, silicon is mostly removed in a ductile model due to the extremely low uncut chip thickness, so the thermal chemical reactions between the diamond tool and the silicon under the high hydrostatic pressure lead to micro-ruggedness of diamond tools. In contrast, the dominant cutting mechanisms in diamond sculpturing is majorly dominated by brittle mode, so the periodic impacts on the apex of the diamond tool highly shorten the tool life and induce the early occurrence of the micro-chipping. Similar results were acquired in slow tool servo of single-crystal silicon [37, 38] and other brittle materials like silicon carbide [39]. Furthermore, the existence of micro-ruggedness increases the sharpness of the diamond tool, accordingly damaging the finished surface with unwanted brittle fractures, as shown in Fig. 17 (b).

It is worth to note that even though the cutting conditions for these two methods are different in the tests, the much deeper cutting depth and the much longer cutting distance adopted in testing of fly cutting indicate more material removal volume. The experiment results demonstrate that compared with the conventional sculpturing method, less tool wear can be achieved by fly cutting even after removing more

material. The enhanced tool life of fly cutting is mainly attributed to its intermittent cutting process with good less heat accumulation in the cutting region as well as less brittle impact on the tool tip.

To further validate superiorities of fly cutting in processing silicon, the SEM images of the tool clearance faces are also measured and shown in Fig. 18. It is observed that obvious nano-grooves are formed on the tool clearance face for sculpturing, as shown in Fig. 18 (a), which is attributed to the abrasive effects of the silicon carbide particles generated by the tribo-chemical reaction between the diamond and silicon [40, 41]. Similar results were also observed in diamond turning of silicon [40]. In comparison, no obvious destruction can be observed on the tool clearance face for fly cutting at this stage, as shown in Fig. 18 (b). Thus, it is learned that the intermittent cutting process of fly cutting is beneficial to enhance tool life in processing brittle materials.

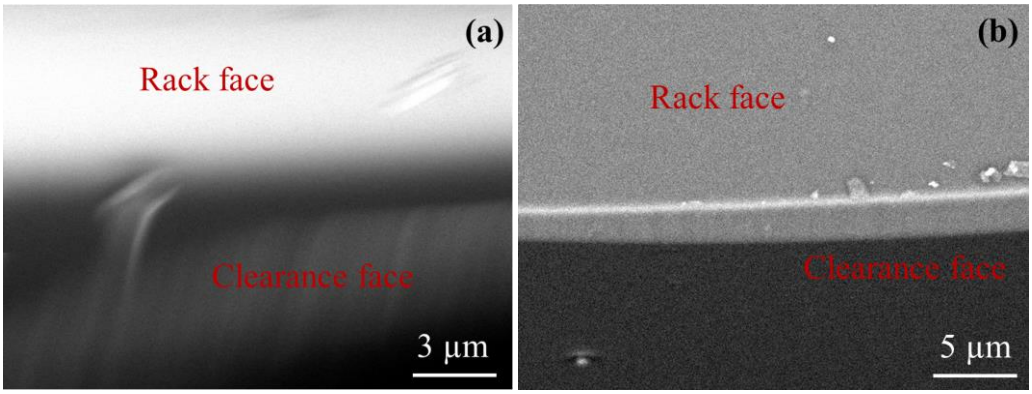

Fig. 18. Tool clearance face for (a) sculpturing and (b) fly cutting.

5. Conclusions

Due to the low fracture toughness of single-crystal silicon, it is a great challenge to effectively obtain deep micro-structures with ultra-smooth surfaces on silicon. Previous research works majorly focus on the fabrication of micro-structures with a small depth (less than 15 μm), but literature on the ductile machining of silicon for deep micro-structures is very limited. In this paper, the feasibility of ultra-precision fly cutting (UPFC) in fabricating deep micro-structures on silicon is demonstrated through modeling and experiments. A novel ductile machining model is first proposed to explain why UPFC can achieve a deep ductile machining depth on silicon, and experimental validation was conducted by fabricating micro-grooves with different depths. The key conclusions are as follows:

(1) The modeling results show that in UPFC, the maximum chip thickness is inversely proportional to the swing radius. Thus, through configuring a large swing radius, the chip thickness will be reduced

to an extremely small value even under large feed rates and depths of cut, thereby ensuring the ductile material removal of silicon for deep micro-structures.

(2) 30 μm deep micro-grooves with a surface roughness of 4 nm Sa were successfully generated by UPFC. In addition, a 15 μm deep micro-raster was also fabricated by UPFC, with a surface roughness of 4 nm Ra and form error of 14 nm PV, fulfilling the requirements for IR applications.

(3) Compared with sculpturing method, much lower ratio of the amorphous silicon was generated by UPFC. Besides, the ratio of the amorphous silicon is not obviously changed in UPFC with increasing depth of cut, due to the small change of the maximum chip thickness in UPFC at different cutting depths.

(4) The maintenance of the ductile machining mechanism in UPFC can prolong the tool life. The tool wear pattern for UPFC shows micro-ruggedness of the tool edge, while the tool wear pattern for sculpturing shows micro-chipping distributed on the tool apex induced by the frequent brittle impact.

Acknowledgement

This work was supported partially by the Research Committee of The Hong Kong Polytechnic University (Project Code: RUNS), Research Grant Council of the Hong Kong Special Administrative Region, China (Project No.PolyU152021/17E), and the National Science Foundation of China (NSFC) (Project No. 51675455).

References

[1] A. Tamang, H. Sai, V. Jovanov, S.I. Bali, K. Matsubara, D. Knipp, On the interplay of interface morphology and microstructure of high-efficiency microcrystalline silicon solar cells, Solar Energy Materials and Solar Cells, 151 (2016) 81-88.

[2] S. John, Why trap light?, Nature Materials, 11 (2012) 997.

[3] G. Dumstorff, C. Pille, R. Tiedemann, M. Busse, W. Lang, Smart aluminum components: Printed sensors for integration into aluminum during high-pressure casting, Journal of Manufacturing Processes, 26 (2017) 166-172.

[4] Y. Wu, L. Zhang, P. Ge, Y. Gao, W. Bi, Effects of the micro-structure of arc-shaped groove, rectangular groove and semicircle-based rectangular groove on the reflectance of silicon solar cell, Solar Energy, 158 (2017) 617-625.

[5] X. Liu, T. Zhou, L. Zhang, W. Zhou, J. Yu, L.J. Lee, Y.Y. Allen, Fabrication of spherical microlens array by combining lapping on silicon wafer and rapid surface molding, Journal of Micromechanics and Microengineering, 28 (2018) 075008.

[6] G. Xiao, S. To, E. Jelenković, Effects of non-amorphizing hydrogen ion implantation on anisotropy in micro cutting of silicon, Journal of Materials Processing Technology, 225 (2015) 439-450.

[7] M.R. Sonne, K. Smistrup, M. Hannibal, J. Thorborg, J. Nørregaard, J.H. Hattel, Modeling and simulation of the deformation process of PTFE flexible stamps for nanoimprint lithography on curved surfaces, Journal of Materials Processing Technology, 216 (2015) 418-429.
[8] Y. He, Y. Yan, Y. Geng, Z. Hu, Fabrication of none-ridge nanogrooves with large-radius probe on PMMA thin-film using AFM tip-based dynamic plowing lithography approach, Journal of Manufacturing Processes, 29 (2017) 204-210.
[9] Y. Pachaury, P. Tandon, An overview of electric discharge machining of ceramics and ceramic based composites, Journal of Manufacturing Processes, 25 (2017) 369-390.
[10] X.-Q. Liu, L. Yu, Z.-C. Ma, Q.-D. Chen, Silicon three-dimensional structures fabricated by femtosecond laser modification with dry etching, Applied optics, 56 (2017) 2157-2161.
[11] R.S. Yadav, V. Yadava, Experimental investigations on electrical discharge diamond peripheral surface grinding (EDDPSG) of hybrid metal matrix composite, Journal of Manufacturing Processes, 27 (2017) 241-251.
[12] Y. Lyu, H. Yu, J. Wang, G. Zhao, Z. Liu, Improved performance of electroplated grinding wheels using a new method of controlled grain size sorting, Journal of Manufacturing Processes, 30 (2017) 336-342.
[13] Z. Sun, S. To, S. Zhang, A novel ductile machining model of single-crystal silicon for freeform surfaces with large azimuthal height variation by ultra-precision fly cutting, International Journal of Machine Tools and Manufacture, (2018).
[14] S. Goel, X. Luo, A. Agrawal, R.L. Reuben, Diamond machining of silicon: a review of advances in molecular dynamics simulation, International Journal of Machine Tools and Manufacture, 88 (2015) 131-164.
[15] Q. Zhang, Y. Fu, H. Su, Q. Zhao, S. To, Surface damage mechanism of monocrystalline silicon during single point diamond grinding, Wear, 396 (2018) 48-55.
[16] J. Xie, Y. Zhuo, T. Tan, Experimental study on fabrication and evaluation of micro pyramid-structured silicon surface using a V-tip of diamond grinding wheel, Precision Engineering, 35 (2011) 173-182.
[17] M. Mukaida, J. Yan, Ductile machining of single-crystal silicon for microlens arrays by ultraprecision diamond turning using a slow tool servo, International Journal of Machine Tools and Manufacture, 115 (2017) 2-14.
[18] D.-H. Choi, J.-R. Lee, N.-R. Kang, T.-J. Je, J.-Y. Kim, E.-c. Jeon, Study on ductile mode machining of single-crystal silicon by mechanical machining, International Journal of Machine Tools and Manufacture, 113 (2017) 1-9.
[19] B.S. Dutterer, J.L. Lineberger, P.J. Smilie, D.S. Hildebrand, T.A. Harriman, M.A. Davies, T.J. Suleski, D.A. Lucca, Diamond milling of an Alvarez lens in germanium, Precision Engineering, 38 (2014) 398-408.
[20] Z. Sun, S. To, S. Zhang, G. Zhang, Theoretical and experimental investigation into non-uniformity of surface generation in micro-milling, International Journal of Mechanical Sciences, 140 (2018) 313-324.
[21] M. Arif, M. Rahman, W.Y. San, An experimental investigation into micro ball end-milling of silicon, Journal of Manufacturing Processes, 14 (2012) 52-61.
[22] P.N. Blake, R.O. Scattergood, Ductile-Regime Machining of Germanium and Silicon, Journal of the American ceramic society, 73 (1990) 949-957.
[23] Y.-L. Chen, Y. Cai, Y. Shimizu, S. Ito, W. Gao, B.-F. Ju, Ductile cutting of silicon microstructures

with surface inclination measurement and compensation by using a force sensor integrated single point diamond tool, Journal of Micromechanics and Microengineering, 26 (2015) 025002.
[24] J. Zhang, J. Zhang, T. Cui, Z. Hao, A. Al Zahrani, Sculpturing of single crystal silicon microstructures by elliptical vibration cutting, Journal of Manufacturing Processes, 29 (2017) 389-398.
[25] H. Mohammadi, D. Ravindra, S.K. Kode, J.A. Patten, Experimental work on micro laser-assisted diamond turning of silicon (111), Journal of Manufacturing Processes, 19 (2015) 125-128.
[26] J. Deng, L. Zhang, J. Dong, P.H. Cohen, AFM-based 3D nanofabrication using ultrasonic vibration assisted nanomachining, Journal of Manufacturing Processes, 24 (2016) 195-202.
[27] J. Wang, P. Feng, J. Zhang, Reducing edge chipping defect in rotary ultrasonic machining of optical glass by compound step-taper tool, Journal of manufacturing Processes, 32 (2018) 213-221.
[28] J. Zhang, N. Suzuki, Y. Wang, E. Shamoto, Fundamental investigation of ultra-precision ductile machining of tungsten carbide by applying elliptical vibration cutting with single crystal diamond, Journal of Materials Processing Technology, 214 (2014) 2644-2659.
[29] S. Zhang, S. To, Z. Zhu, G. Zhang, A review of fly cutting applied to surface generation in ultra-precision machining, International journal of machine tools and manufacture, 103 (2016) 13-27.
[30] Z. Sun, S. To, K. Yu, One-step generation of hybrid micro-optics with high-frequency diffractive structures on infrared materials by ultra-precision side milling, Optics Express, 26 (2018) 28161-28177.
[31] R. Komiya, T. Kimura, T. Nomura, M. Kubo, J. Yan, Ultraprecision cutting of single-crystal calcium fluoride for fabricating micro flow cells, Journal of Advanced Mechanical Design, Systems, and Manufacturing, 12 (2018) JAMDSM0021-JAMDSM0021.
[32] Y. Peng, T. Jiang, K. Ehmann, Research on single-point diamond fly-grooving of brittle materials, The International Journal of Advanced Manufacturing Technology, 75 (2014) 1577-1586.
[33] J. Yan, T. Asami, H. Harada, T. Kuriyagawa, Fundamental investigation of subsurface damage in single crystalline silicon caused by diamond machining, Precision Engineering, 33 (2009) 378-386.
[34] J.E. Harvey, N. Choi, S. Schroeder, A. Duparré, Total integrated scatter from surfaces with arbitrary roughness, correlation widths, and incident angles, Optical Engineering, 51 (2012) 013402.
[35] H. Ottevaere, R. Cox, H.-P. Herzig, T. Miyashita, K. Naessens, M. Taghizadeh, R. Völkel, H. Woo, H. Thienpont, Comparing glass and plastic refractive microlenses fabricated with different technologies, Journal of Optics A: Pure and Applied Optics, 8 (2006) S407.
[36] J. Yan, T. Asami, T. Kuriyagawa, Nondestructive measurement of machining-induced amorphous layers in single-crystal silicon by laser micro-Raman spectroscopy, Precision Engineering, 32 (2008) 186-195.
[37] X. Li, T. He, M. Rahman, Tool wear characteristics and their effects on nanoscale ductile mode cutting of silicon wafer, Wear, 259 (2005) 1207-1214.
[38] M.S. Uddin, K. Seah, X. Li, M. Rahman, K. Liu, Effect of crystallographic orientation on wear of diamond tools for nano-scale ductile cutting of silicon, Wear, 257 (2004) 751-759.
[39] J. Yan, Z. Zhang, T. Kuriyagawa, Effect of Nanoparticle Lubrication in Diamond Turning of Reaction-Bonded SiC, IJAT, 5 (2011) 307-312.
[40] W. Zong, T. Sun, D. Li, K. Cheng, Y. Liang, XPS analysis of the groove wearing marks on flank face of diamond tool in nanometric cutting of silicon wafer, International Journal of Machine Tools and Manufacture, 48 (2008) 1678-1687.
[41] C. Pantea, Kinetics of diamond-silicon reaction under high pressure-high temperature conditions, 2004.